Applied Catalysis B: Environmental 183 (2016) 142–148

Contents lists available at ScienceDirect

Applied Catalysis B: Environmental

journal homepage: www.elsevier.com/locate/apcatb

Cs_xWO_3 nanorods: Realization of full-spectrum-responsive photocatalytic activities from UV, visible to near-infrared region

Guilian Li[a,b], Chongshen Guo[a,*], Mei Yan[a], Shaoqin Liu[a,*]

[a] Key Lab of Microsystem and Microstructure (Ministry of Education), Harbin Institute of Technology, No. 2 YiKuang Street, Harbin 150080, China
[b] Department of Environmental Science and Engineering, Heilongjiang University, Harbin 150080, China

ARTICLE INFO

Article history:
Received 16 September 2015
Received in revised form 10 October 2015
Accepted 18 October 2015
Available online 21 October 2015

Keywords:
Tungsten bronze
Full-spectrum-response photocatalysis
Cs_xWO_3
Near infrared

ABSTRACT

Effective utilization of solar energy in photocatalytic materials is one of most essential issues what the photochemists are very concerned all along. In this work, full-spectrum-response photocatalytic activities covering UV, visible and near infrared regions on degradation of methylene blue have been realized firstly on single matter of the mixed valence $Cs_{0.32}WO_3$ nanorod. As revealed by optical absorption results, advantages of $Cs_{0.32}WO_3$ nanorod used in this purpose originated from its high optical absorption in the whole solar spectrum of 300–2500 nm. Benefitting from this unique photo-absorption property, the photocatalytic property of Cs_xWO_3 nanorod displayed a significant advance in fully utilization of all solar energy, especially for NIR part, which holds considerable percentage of sunlight but seldom is utilized up to now. The removal rates of MB on Cs_xWO_3 nanorod were determined to be 72, 70 and 37% under 185 mw/cm^2 UV, 166 mw/cm^2 visible and 42.7 mW/cm^2 NIR irradiation within the test duration, respectively. In addition, a plausible mechanism toward understanding the near-infrared driven photocatalytic activity on $Cs_{0.32}WO_3$ nanorod has been proposed on the basis of ESR results and polaron absorption theory.

1. Introduction

Sunlight is a portion of the electromagnetic radiation given off by the Sun, in particular infrared, visible, and ultraviolet light [1,2]. If people carefully check the spectrum of the solar radiation, it is easily to find that the sunlight arriving at the earth's surface is around 52 or 55% near infrared (above 700 nm), 43 or 42% visible light (Vis, 400–700 nm), and 5 or 3% ultraviolet (UV, below 400 nm) in terms of energy. How to make the utmost use of solar energy to serve for the human life has been an interesting challenge for the scientists. Over the past decades, the UV and visible light have been intensively utilized to serve for photocatalytic reactions [3–5], solar cells [6–8], solar heater [9] and so forth. Compared with efforts on making use of the visible light or UV light, studies relating to exploiting near-infrared light (NIR), which takes up to about half of sunlight, are rather rare.

Photocatalysis for the removal of organic pollutants is a precise example on this point. It is well-known that photocatalytic degradation process is the most studied ones and considered to be efficient and economical purification method on account of their simple procedures, ambient operating conditions, green and lower costs [10,11]. However, removal of organic pollutants from wastewater through photocatalytic degradation process also suffers drawbacks of insufficient utilization on solar energy. As far as light-harvesting is concerned, most of efforts have been focused on extending the photo-responsive region of photocatalyst to match the utmost of solar energy. The landmark cases, such as N-doped TiO_2 photocatalysts [12,13], plasmonic photocatalysts [14,15], and dye-sensitized photocatalysts [16–17], were developed to make the photocatalysts to be effective under visible light. What is a pity, despite all these advances, the near-infrared light remains seldom being utilized. To the best of our knowledge, only several kinds of nanomaterials, including up-conversion photocatalyst, Bi_2WO_6/TiO_2 and $Cu_2(OH)PO_4$, have tentatively been employed as NIR-driven photocatalyst until now [18–21], and the aim to discover a full-spectrum-responsive photocatalyst is far from being realized. We take the up-conversion composited photocatalyst for example, it can convert NIR light to visible or UV light and then transfer energy to UV or visible light active photocatalysts to induce a photocatalytic effect. However, the quantum efficiency of composited up-conversion photocatalyst is much low and the excitation source is limited to 980 nm. As a result, realization of full-

* Corresponding author at: Room404, Building No.B1, Yikuang Street No.2, Science Park of Harbin Institute of Technology, Harbin, China.
E-mail addresses: chongshenguo@hit.edu.cn, bigguop@mail.tagen.tohoku.ac.jp (C. Guo), shaoqinliu@hit.edu.cn (S. Liu).

http://dx.doi.org/10.1016/j.apcatb.2015.10.039
0926-3373/

spectrum-responsive photocatalytic activities by single species has not been investigated yet further.

For realizing the aimed full-spectrum-responsive photocatalytic properties, a broadband absorptive ability is a prerequisite for the photocatalyst. Early on, we have successfully exploited the synthesis of homogeneous tungsten bronze type nanocrystals of Cs_xWO_3, which consists of mixed chemical valence tungsten ions of W^{6+} and W^{5+} [22,23]. More importantly, the tungsten bronze type nanocrystals of Cs_xWO_3 exhibit strong optical absorption in a wide range of 200~2500 nm, covering the waveband of UV, visible and whole NIR region. Can we extend the application of Cs_xWO_3 nanorod into the photocatalytic research and achieve a full-spectrum-responsive photocatalytic effect on this single matter, instead of composited materials? In this work, we present the feasibility of realizing the advanced full-spectrum-responsive photocatalytic activity by Cs_xWO_3 nanorod only, which has never been studied as photocatalyst before this work.

2. Experimental

2.1. Materials

All the chemicals were of analytical grade and used without further purification. The tungsten hexachloride (WCl_6), $CsOH{\cdot}H_2O$, dehydrated ethanol and acetic acid were purchased from Kanto Chemical Co., Inc.

2.2. Synthesis of Cs_xWO_3 nanorods

In a typical experiment, 0.2976 g WCl_6 was dissolved into the 40 mL dehydrate ethanol under violently stirring. Then, 0.065 g $CsOH{\cdot}H_2O$ was introduced to the above yellowish solution. After the mixture become homogeneous, 10 ml acetic acid was added. The final concentration of WCl_6 was 0.015 M and nominal Cs/W atomic ratio was 0.5. After that, the mixture solution was transferred into a Teflon-lined autoclave of 100 mL internal volume, followed by solvothermal treatment at 240 °C for 20 h. After the reaction, the dark blue powder was centrifuged and washed with water and ethanol for many times, and then finally dried in vacuum at 60 °C [23].

2.3. Characterization

The phase composition of the sample was determined by X-ray diffraction analysis (XRD, Shimadzu XD-D1) using graphite-monochromized CuKα radiation. The nanostructure of the sample was observed by a transmission electron microscope (TEM, JEOLJEM-2010). HRTEM images were obtained on a ZEISS LEO 922 with an accelerating voltage of 200 kV. The surface composition and W_{4f} binding energy of the sample were determined by X-ray photoelectron spectroscopy (XPS, Perkin Elmer PHI 5600). The optical properties were measured using a spectrophotometer (U-4100. Hitachi), giving an output of transmittance in the UV, visible, and infrared ranges (200–3300 nm). The thermogravimetric analysis (TG, Rigaku, TG8101D) was performed for the sample from room temperature to 900 °C with a heating rate of 10 °C/min in the air. X-band electron spin resonance (ESR) spectra were recorded on an ER-300 ESR spectrometer (Burker Instruments Inc.) with a modulation frequency of 100 kHz. The center field was 3570 G, and the sweep width was 73 G.

2.4. Photocatalytic test

The full-spectrum-responsive photocatalytic activity of Cs_xWO_3 nanorod was investigated by the photodegradation of methyl blue (MB, 50 mg/L). During the test, it was found that there was a strong electrostatic attraction between MB molecules and Cs_xWO_3 nanorod, and the maximum uptake of MB determined according to Langmuir adsorption model was 56 mg g^{-1}. To eliminate the influence of absorption on the experimental results, 0.1 g Cs_xWO_3 powder was pre-saturated in 50 mL 100 mg L^{-1} MB solution to reach a absorption–desorption equilibrium firstly, and then the photocatalyst of Cs_xWO_3 was centrifuged and transferred to reactant MB solution of 50 mg L^{-1}. Moreover, prior to light irradiation, the suspensions were magnetically stirred in the dark for 30 min to establish adsorption–desorption equilibrium further. A 300 W Xe arc lamp was used as the UV or visible light source under assistance of filters to assure the light < 400 nm as UV source and light of 400–800 nm as visible source. In addition, a 200 W infrared lamp was employed as the near infrared source and lights < 800 nm were cut off by filter. At varied irradiation time intervals, 2 mL mixed solution was collected and centrifuged, and the residual MB concentration was determined by UV–vis spectroscopic measurements (Hitachi U-4100).

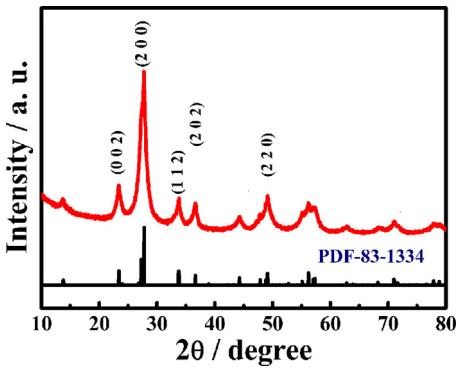

Fig. 1. The XRD pattern of Cs_xWO_3 sample. (Reference: $Cs_{0.33}WO_3$, JCPDS No. 83-1334).

3. Results and discussion

3.1. Characterizations on Cs_xWO_3 nanocrystals

Firstly, we investigated the crystal phase of obtained powder sample by XRD analysis. Fig. 1 displays the typical XRD pattern of as-synthesized blue powders resulting from the solvothermal reaction at 240 °C for 24 h. It can clearly be seen that all of the reflective peaks could be well indexed to hexagonal cesium tungsten bronze (JCPDS No. 831334) and no impurity peaks were identified. In addition, the intensity of these XRD peaks was relative weak and half-peak breadth was wide, being consistent with the general features of the nanoparticles. Enlighten by this, the average crystallite size (D) of the sample was calculated to be 65 nm using the well-known Scherrer equation:

$$D = \frac{K\lambda}{\beta\cos(\theta)} \quad (1)$$

where λ is the wavelength of the X-ray radiation ($\lambda = 0.15418$ nm), K is the Scherrer constant ($K = 0.89$), θ is the Bragg angle of the X-ray diffraction peak, and β is the line broadening at half the maximum intensity (FWHM, in radians) of the (2 0 0) plane of Cs_xWO_3 sample.

Later, the nanostructure characters of Cs_xWO_3 sample were examined by HR-TEM technique. Fig. 2a and b shows the typical morphology of Cs_xWO_3 nanostructure selected in this work. The sample is observed to be homogeneous rod-like particles with diameter in 5–8 nm and length up to 40–60 nm, being in accordance with calculated XRD result of 65 nm. The chemical composition analysis based on the EDS-mapping indicates that these nanorods are composed of Cs, O and W elements (Fig. 2c–e), and

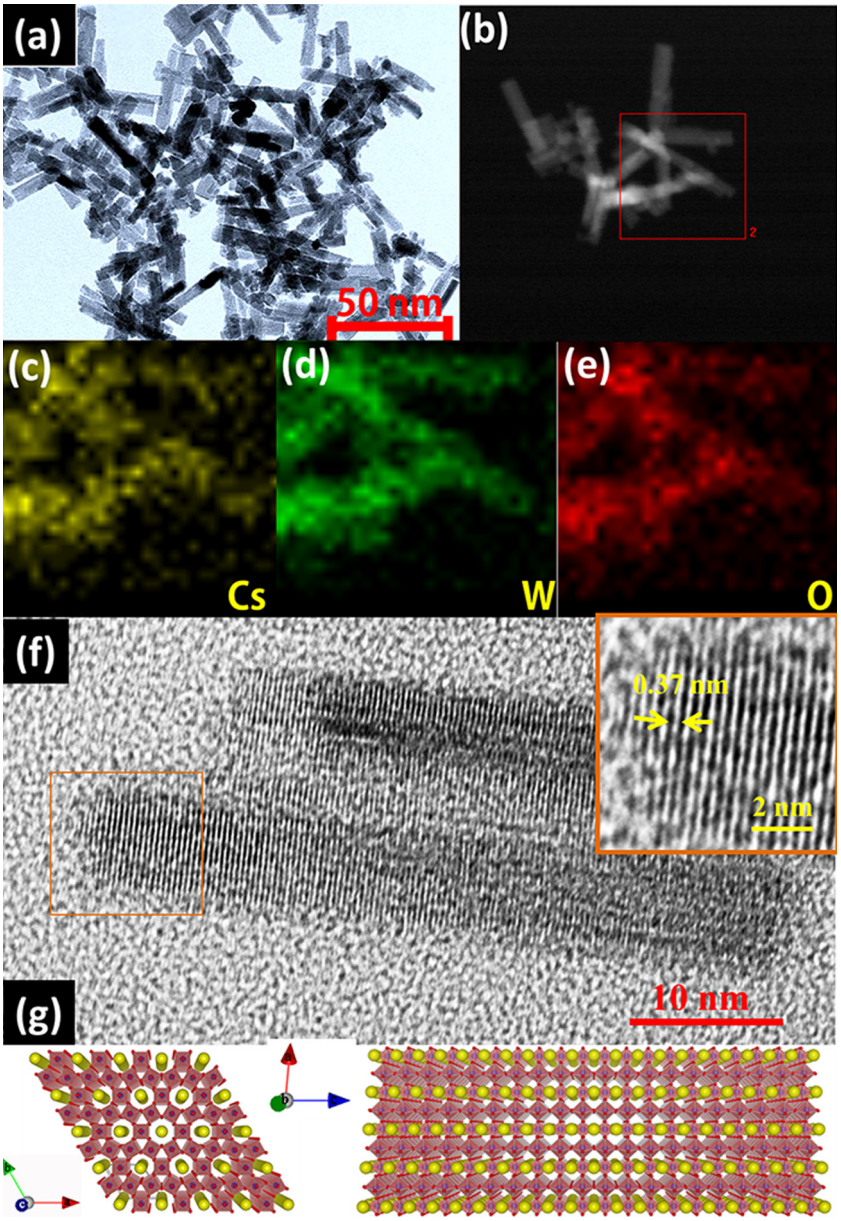

Fig. 2. (a) TEM image, (b) HAADF-STEM image, (c–e) elemental EDS-mapping image of Cs_xWO_3 nanorods. (the rectangle inside the Fig. 2b is the EDS-mapping area); (f) HR-TEM image and (g) crystal structure of Cs_xWO_3 nanorods view from *c* and *b* plane direction. (For interpretation of the references to color in this figure legend, the reader is referred to the web version of this article.)

the atomic ratio of Cs:W is further determined to be 0.32, which is very close to the theoretical maximum of 0.33. In addition, all the phases of hexagonal Cs_xWO_3 with x in the range of 0–0.33 show nearly the same XRD pattern to each other, and the only difference between them is sight shift of 2θ in the XRD pattern. In this regard, although the XRD pattern of our sample is close to standard phase of $Cs_{0.33}WO_3$, we attributed our sample to the $Cs_{0.32}WO_3$ on the basis of more accurate EDX results. A magnified observation on HR-TEM image of two Cs_xWO_3 nanorods, shown in Fig. 2f, shows clear and ordered lattice fringes, suggesting that these nanorods are single crystal. What is more, the well-defined lattice fringe within the nanorods and with a spacing of 0.37 nm agreed well with (0 0 2) spacing of $Cs_{0.32}WO_3$, indicating a preferential growth along the *c*-axis of the hexagonal bronze structure. For the hexagonal tungsten bronzes (M_xWO_3, $x \leq 0.33$), the structure mainly comprises a rigid tungsten-oxygen framework built up of layers containing corner-sharing WO6 octahedron, which are arranged in 6 membered rings. The layers are stacked along the *c*-axis, leading to the formation of one-dimensional open hexagonal channels, which are occupied randomly by cations (Fig. 2g) [24]. Therefore, growth habit prefers to occur along the *c*-axis of Cs_xWO_3 nanorod according to its specific crystal structure.

As reported previously, the W ions in the tungsten bronze of Cs_xWO_3 (which could be exactly expressed as $Cs_xW_x^{5+}W_{1-x}^{6+}O_3$) should be a mixture of W^{+6} and W^{+5} ions [1,2,22,23]. To check the chemical valence of sample, XPS analysis was performed on the core-level of W 4f. The obtained XPS curve could be fitted into two spin-orbit doublets, corresponding to two different oxidation states of W atoms (Fig. 3). The main peaks, having a W $4f_{5/2}$ at 37.5 eV and a W $4f_{7/2}$ at 35.4 eV, could be attributed to the W atoms being in a +6 oxidation state. The second doublet, with a lower binding energy at 34.4 eV and 36.5 eV, could be ascribed to the emission of W$4f_{5/2}$ and W$4f_{7/2}$ core levels from the W atoms in an oxidation state of 5+.

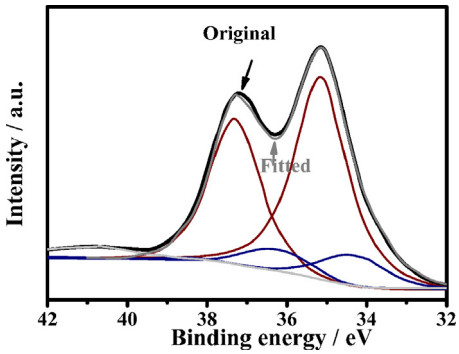

Fig. 3. Deconvolution of W4f core-level spectrum with peaks corresponding to W^{6+} and W^{5+} oxidation states.

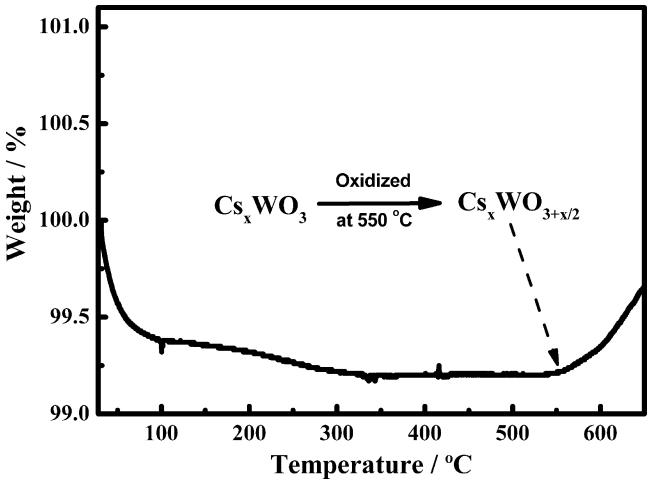

Fig. 4. Thermogravimetric curve of as-synthesized Cs_xWO_3 nanorods heated in the air, which shows an obvious oxidization at 550 °C. The test was performed with a heating rate of 10 °C/min.

Taken above XRD, EDS and XPS results together, it can firmly conclude that the nanorod used in this work is a tungsten bronze phase of $Cs_{0.32}WO_3$.

Considering that the chemical or thermal stability of low-valence W^{5+} ions is a significant criterion for the photocatalytic application and long-term storage, the thermal behavior of as-prepared Cs_xWO_3 nanorods was investigated via thermogravimetry measurement in an air atmosphere at a heating rate of 10 °C/min. As shown in Fig. 4, there are 3 stages of obvious weight changes, that are, weight loss at 30–100 °C and 100–250 °C, as well as weight increment above 550 °C. Firstly, the weight loss up to about 250 °C might be attributed to the desorption of water, including the loss of surface adsorbed water (~100 °C) and structural water elimination (~250 °C). Secondly, the obvious weigh increment above 550 °C could be well assigned to the oxidation process of the cesium tungsten bronze by air oxygen above a certain temperature as a result of conversion from W^{5+} to W^{6+}. What is noteworthy, the sample after TG test shows a faint yellow color, instead of deep blue for as-obtained Cs_xWO_3 nanorods.

$$Cs_xWO_3 + \frac{x}{4O_2} = Cs_xWO_{3+x/2} \quad (2)$$

On the basis of TG results, it can conclude that the Cs_xWO_3 nanorod is of adequate stability and the W^{5+} ions could be maintained even under heating in air if the temperature is below 550 °C. What is more, a long-term observation on Cs_xWO_3 nanorod indicates an excellent chemical stability of Cs_xWO_3 nanorod under ambient conditions. The stored Cs_xWO_3 nanorod synthesized three years ago is exhibiting same chemical valence state, crystal phase, nanostructure as just obtained.

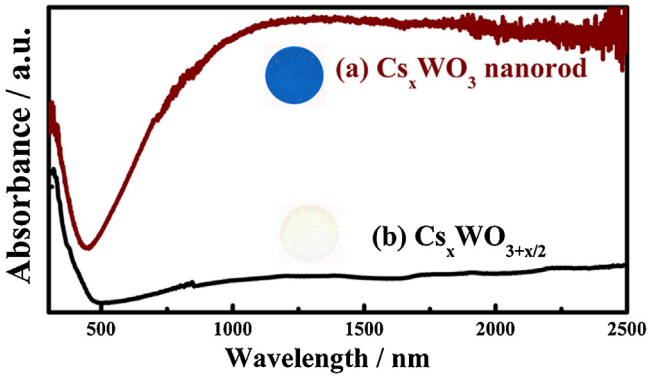

Fig. 5. Powder absorbance spectra of (a) Cs_xWO_3 nanorods and (b) control of $Cs_xWO_{3+x/2}$. The inset also shows the corresponding colors for samples. (For interpretation of the references to color in this figure legend, the reader is referred to the web version of this article.)

The optical absorptive property is another critical factor on determining whether certain material is a potential candidate as photocatalysis, the powder absorbance spectra of Cs_xWO_3 nanorods were measured and shown in Fig. 5a. It clearly reveals that the blue powder of Cs_xWO_3 nanorod exhibits obvious optical absorption in the whole solar region of 300–2500 nm, especially for the NIR light of 780–2500 nm, which is highly necessary for investigating the aimed full-spectrum-response photocatalytic activity. Until now, although the reason why tungsten bronzes can give a strong and wide absorption in the NIR area has not been well elucidated yet, it was thought to be related to W^{5+} induced the plasmon resonance of free electrons, interband transition and small polarons in previous work [25–27]. An excellent photocatalytic activity is expected as it has been reported recently that W^{5+} plays an important role in photocatalytic process [28–30]. If the Cs_xWO_3 is calcined in the air above 650 °C to form fully oxidized $Cs_xWO_{3+x/2}$, the prominent absorption of NIR light disappeared and only a bandgap excitation at about 500 nm was observed (Fig. 5b), suggesting that the contribution of NIR absorption comes from chromophore of low-valence W^{5+}. In addition, the deep blue of Cs_xWO_3 turned to be pale yellow after oxidized into $Cs_xWO_{3+x/2}$ as shown in Fig. 5 inset.

3.2. Photocatalytic performance of Cs_xWO_3

To check the intrinsic photocatalytic activity of Cs_xWO_3 nanorods, the 0.1 g catalyst was pre-saturated in a MB solution with a concentration of 100 mg L^{-1} to reach a absorption–desorption equilibrium, and then centrifuged and transferred to another MB solution of 50 mg L^{-1} for photocatalytic reaction. This process taken was in consideration of high absorption capacity of Cs_xWO_3 nanorods. A 300 W Xe arc lamp was used as the UV or visible light source under assistance of filters to assure the light < 400 nm as UV source and light of 400–800 nm as visible source. In addition, a 200 W infrared lamp was employed as the near infrared source and lights < 800 nm were cut off. As shown in Fig. 6A, the Cs_xWO_3 nanorods exhibit prominent photocatalytic activities on decoloration of MB molecules under partitioned spectrum of UV, visible, and even NIR irradiation. The removal rate of MB are determined to be 72, 70 and 37% under 185 mw/cm^2 UV, 166 mw/cm^2 visible and 42.7 mW/cm^2 NIR irradiation, respectively. As well known that water can also absorb the NIR light > 1400 nm, it maybe convert the NIR light into the local heat and lead to a thermolysis on MB species. To eliminate such an effect, besides employing cycle cooling water in the reactor, the control test of destruction on MB by only NIR

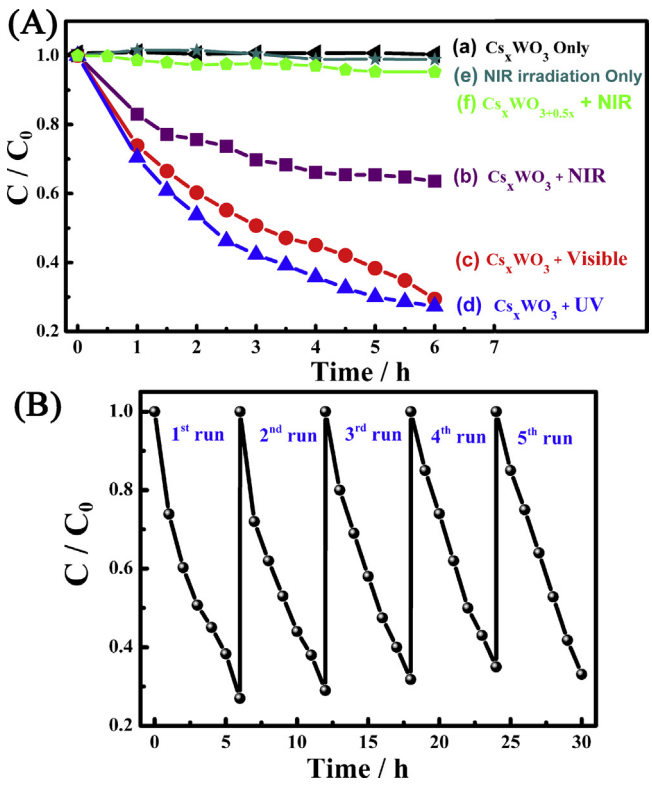

Fig. 6. Photocatalytic activity in degradation of MB under conditions of (a) only Cs_xWO_3 without light irradiation, (b) Cs_xWO_3 + NIR light irradiation (>800 nm), (c) Cs_xWO_3 + visible light (400–800 nm), (c) Cs_xWO_3 + UV light (<400 nm) irradiation, (e) NIR irradiation only, (f) $Cs_xWO_{3+x/2}$ + NIR light irradiation (>800 nm), respectively. (B) Recycling stability of $Cs_{0.32}WO_3$ under visible light irradiation.

Table 1
TOC, TC and IC values of solutions after UV, visible and NIR irradiation, respectively (unit: mg/L).

Sample	TOC	TC	IC
Initial solution (before reaction)	27.31	27.91	0.60
NIR irradiation for 6 h	22.38	23.08	0.70
Visible light irradiation for 6 h	19.95	26.20	6.25
UV irradiation for 6 h	16.03	16.60	0.57

irradiation or photocatalyzed by fully oxidized $Cs_xWO_{3+x/2}$ is carried out as well. The results reveal that both of them account for a negligible decolorization rate on MB. As a result, it further confirms the NIR-driven photocatalytic property of Cs_xWO_3 nanorods. Taken together, Cs_xWO_3 nanorod is potential photocatalyst with full-spectrum-response photocatalytic properties, which benefits from its wide and strong absorption spectrum across from UV to NIR. To investigate the recycling stability of $Cs_{0.32}WO_3$, the cycling of photodegradation on MB under visible light was tested. As is shown in Fig. 6B, the $Cs_{0.32}WO_3$ shows adequate recycling stability and there is negligible deterioration on photocatalytic activity after 5 cycles.

In order to investigate the mineralizing ability of $Cs_{0.32}$ WO_3, the total organic carbons (TOCs), total organic carbons (TC) and inorganic carbons (IC) analysis on the degraded solutions are measured. From Table 1 we can see that the TOC values obviously decreased after irradiation by either UV, visible or NIR light. By calculating on the TOC value, 41, 27, 18% of TOC is confirmed to be mineralized to CO_2 under UV, visible and NIR light irradiation, respectively. This result demonstrates that the $Cs_{0.32}WO_3$ nanorods possess favorable mineralizing ability.

3.3. Full-spectrum-responsive photocatalytic degradation mechanism of Cs_xWO_3

Early on, photocatalytic degradation mechanism of dye under the UV or visible light irradiation on semiconductors has been well established as an oxidative process in which three consecutive steps are involved. Firstly, light with higher energy than badgap of semiconductor is absorbed and afterwards induces a transition of electrons from the valence band to the conduction band, leaving an equal number of holes in the valence band. Secondly, the excited electrons and holes migrate to the surface. Thirdly, the superficial photogenerated electron–hole pairs produce several reactive intermediate species for destruction of dye molecules. Generally, the photogenerated electrons are scavenged by dissolved oxygen, and then superoxide ($O_2^{\bullet -}$) would be obtained first, followed by formation of other reactive oxygen species including hydroperoxyl radical (HOO•), H_2O_2, or hydroxy radical (OH•) [31]. All these reactive oxygen species possess sufficient energy for oxidation of pollutants. In our case, owing to a badgap excitation edge at 500 nm of Cs_xWO_3 (Fig. 5a), above-mentioned general mechanism can well make an explanation on the photocatalytic activity of Cs_xWO_3 under UV or shortwave visible irradiation.

In this study, we are more concerned about the mechanism of NIR-driven photo-degradation by Cs_xWO_3 nanorod, which has never been touched. To tentatively confirm it, the actual reactive oxidizing species in the catalytic oxidation process under NIR irradiation were detected by ESR spectroscopy.

Firstly, ESR spectroscopy was used to detect •OH in the catalytic system. As shown in Fig. 7a, a quartet of signals from the DMPO-•OH adducts with relative intensities of 1:2:2:1 were detected after exposure to NIR irradiation for 45 min, illustrating that •OH was formed during the photocatalytic reaction process [32]. What is in a sharp contrast is that there is no detectable signal for the group in the dark. Moreover, the generation of singlet oxygen ($^1O_2$) under NIR irradiation was checked by the detection of TEMPO, which is a product of reaction between TEMP and $^1O_2$ in situ [33,34]. In Fig. 7b, all the signals could be assigned to the TEMPO standard, indicating the generation of $^1O_2$ either in the dark or under NIR condition. However, the relative intensities of TEMPO signal under NIR irradiation were much higher than that in the dark, suggesting the NIR irradiation could efficiently enhance the production of $^1O_2$.

On the basis of all the information above, a plausible mechanism is proposed to explain the reasons why Cs_xWO_3 can give a NIR-driven photocatalytic activity. When Cs_xWO_3 nanorod was subjected to the NIR irradiation, W^{5+} sites as chromophore or photosensitive sites were excited with photogenerated electrons and W^{6+} produced (Eq. (3)). This phenomenon is a similar case to that of reported $Cu_2(OH)PO_4$, where valence alternation of Cu ions was considered to induce extinction of NIR light and play an important role on NIR-driven photocatalytic activity [21]. Subsequently, photogenerated electrons could be trapped by absorbed O_2 to form $^-O_2$, followed by the generation of •OH, •OOH and $^1O_2$ (Eqs. (4) and (5)) [35]. On the other side, the W^{6+} sites can react with OH^- and return to W^{5+}, realizing a full photocatalytic circle. Finally, the reactive species, including •OH, •OOH and $^1O_2$ all possess sufficient energy for oxidation of dyes (Eq. (7)).

$$W^{5+} + h\nu(\mathrm{NIR}) \rightarrow W^{6+} + e^- \quad (3)$$

$$e^- + O_2 \rightarrow {}^{\bullet}O_2^- + H^+ \rightarrow {}^{\bullet}OOH \rightarrow\rightarrow {}^{\bullet}OH \quad (4)$$

$${}^{\bullet}O_2^- + {}^{\bullet}OH \rightarrow {}^1O_2 + OH^- \quad (5)$$

$$W^{6+} + OH^- \rightarrow W^{5+} + {}^{\bullet}OH \quad (6)$$

$${}^{\bullet}O_2^-, {}^{\bullet}OH, {}^1O_2 + \mathrm{MB} \rightarrow \mathrm{DegradationofMB} \quad (7)$$

The mechanism of NIR absorbing by tungsten bronzes can provide the theoretical support on happening of reaction shown in

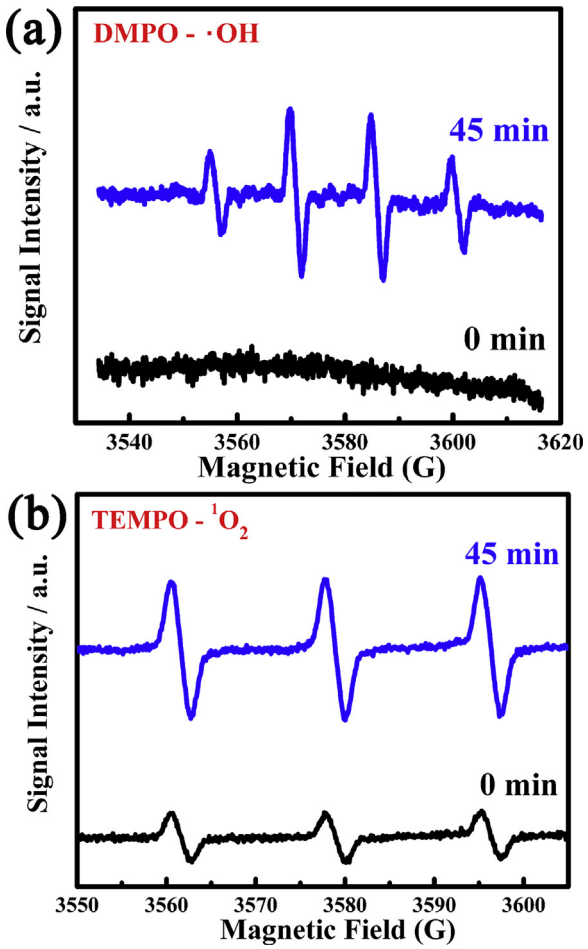

Fig. 7. ESR spectra of (a) the DMPO adduct with •OH and (b) the TEMP adduct with $^1O_2$ generated under NIR irradiation in the reaction system.

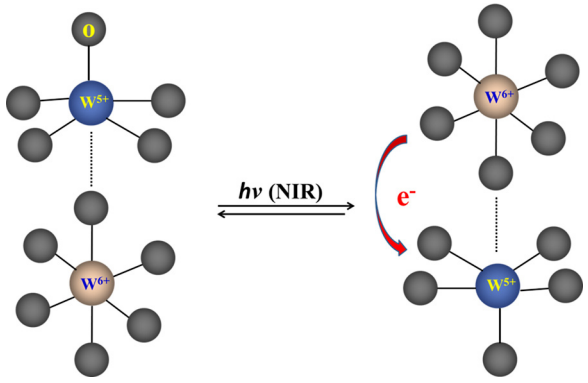

Fig. 8. Schematic diagram of polaron hopping between the W^{6+} and W^{5+} states.

Eq. (3). Inter-valence charge transfer and small polaron absorption theories are the most widely accepted two models to explain the mechanism of NIR absorption by reduced tungsten oxides [25,26]. Above-mentioned two theories have been well established via both experimental evidences and theoretical calculations in other's previous work. To put the essences of these two models simply, the absorption of NIR light is considered to be the polaron transfer by hopping between two neighboring nonequivalent tungsten sites (see Fig. 8, Eq. (8)), denoted as A and B, as follows:

$$h\nu + W^{5+}(A) + W^{6+}{}_{(B)} \rightarrow W^{6+}{}_{(A)} + W^{5+}{}_{(B)} + E_{phonon} \quad (8)$$

where E_{phonon} represents single phonon energy.

In other pellucid words, the NIR light irradition on Cs_xWO_3 induces one electron to escape from its W^{5+} site and then oxidizes the original W^{5+} into W^{6+}, which is exactly in accordance with the essence of Eq. (3) we proposed. If system is only composed of nanocrystals of reduced tungsten oxides, the only way where this electron to go is another adjacent W site, resulting in formation of a new W^{5+} site. However, in our case of photocatalytic reaction in the aqueous dye solution, another way for the NIR induced free electrons is scavenged by dissolved oxygen to produce various reactive species as Eqs. (4) and (5). Therefore, the proposed photocatalytic mechanism (as shown in Eqs. (3)–(7)) can give a sound explanation on why Cs_xWO_3 can give a NIR-driven photocatalytic activity.

Finally, W^{5+} ions may also be excited by visible light of >500 nm (which is unable to induce a badgap excitation) in a similar way to that of Eq. (3), and resultantly account for part of visible light driven photocatalytic activity.

4. Conclusions

In this study, we successfully realized full-spectrum-responsive photocatalytic activities by single matter of $Cs_{0.32}WO_3$ nanorod, which is an excellent optical absorber that can prominently harvest the light in a wide range of 300–2500 nm. The experimental results confirmed that the low-valance W^{5+} sites are the origin of NIR absorption, also upon which the free electrons could be generated under the NIR irradiation and subsequently formed reactive oxygen species for photodegradation of MB molecules. ESR results provided strong experimental evidence to the generation of reactive oxygen species and the polaron absorption theory gave a theoretical support on release of free electrons from W^{5+} sites as NIR irradiation. Taken them together, a photocatalytic mechanism under NIR irradiation was well established. Finally, our work suggests that it will be promising to use this tungsten bronze nanomaterial for efficiently removal of organic dyes under any part of solar light available, whether UV, visible or near infrared light. This work realized utmost match of solar energy for the aimed photocatalytic reaction.

Acknowledgements

The financial supports from the National Natural Science Foundation of China (Grant No. 21303033, 81373359 and 51572059) are gratefully acknowledged. This work is also supported by the "Fundamental research Funds for the Central Universities" (Grant No. HIT. NSRIF.2015061), Heilongjiang Postdoctoral Financial Assistance (Grant No. LBH-Z13079) and China Postdoctoral Science Foundation Funded Project (Project No.2014M551232).

References

[1] C.S. Guo, S. Yin, Q. Dong, T. Sato, Nanoscale 4 (2012) 3394–3398.
[2] C.S. Guo, S. Yin, L.J. Huang, T. Sato, ACS Appl. Mater. Interfaces 3 (2011) 2794–2799.
[3] D. Gregori, C. Guillard, I. Benchenaa, D. Leonard, S. Parola, Appl. Catal. B 176–177 (2015) 472–479.
[4] V. Vaiano, O. Sacco, G. Iervolino, D. Sannino, P. Ciambelli, R. Liguori, E. Bezzeccheri, A. Rubino, Appl. Catal. B 176–177 (2015) 594–600.
[5] C. Belver, J. Bedia, J.J. Rodriguez, Appl. Catal. B 176–177 (2015) 278–287.
[6] Q. Li, X. Jin, X. Yang, C. Chen, Z. Chen, Y. Qin, T. Wei, W. Sun, Appl. Catal. B 162 (2015) 524–531.
[7] J.H. Seo, D. Kim, S. Kwon, M. Song, M. Choi, S.Y. Ryu, H.W. Lee, Y. Chang Park, J.D. Kwon, K. Nam, Y. Jeong, J. Kang, C.S. Kim, Adv. Mater. 24 (2012) 4523–4527.
[8] M.M. Lee, J. Teuscher, T. Miyasaka, T.N. Murakami, H.J. Snaith, Science 2 (2012) 643–647.
[9] E. Halawa, K.C. Chang, M. Yoshinaga, Renew. Energy 83 (2015) 1279–1286.
[10] X. Ma, H. Li, Y. Wang, H. Li, B. Liu, S. Yin, T. Sato, Appl. Catal. B 158–159 (2014) 314–320.
[11] H. Li, S. Yin, Y. Wang, T. Sato, Appl. Catal. B 132–133 (2013) 487–492.

[12] G.D. Yang, Z. Jiang, H.H. Shi, T.C. Xiao, Z.F. Yan, J. Mater. Chem. 20 (2010) 5301–5309.
[13] M. Mrowetz, W. Balcerski, A.J. Colussi, M.R. Hoffman, J. Phys. Chem. B 108 (2004) 17269–17273.
[14] X. Zhang, X. Ke, A. Du, H. Zhu, Sci. Rep. 4 (2014) 3805.
[15] Z. Lian, W. Wang, S. Xiao, X. Li, Y. Cui, D. Zhang, G. Li, H. Li, Sci. Rep. 5 (2015) 10461.
[16] T. Kajiwara, K. Hashimoto, T. Kawai, T. Sakata, J. Phys. Chem. 86 (1982) 4516–4522.
[17] T. Shimidzu, T. Iyoda, Y. Koide, J. Am. Chem. Soc. 107 (1985) 35–41.
[18] W. Qin, D. Zhang, D. Zhao, L. Wang, K. Zheng, Chem. Commun. 46 (2010) 2304–2306.
[19] Z.X. Li, F.B. Shi, T. Zhang, H.S. Wu, L.D. Sun, C.H. Yan, Chem. Commun. 47 (2011) 8109–8111.
[20] J. Tian, Y. Sang, G. Yu, H. Jiang, X. Mu, H. Liu, Adv. Mater. 25 (2013) 5075–5080.
[21] G. Wang, B. Huang, X. Ma, Z. Wang, X. Qin, X. Zhang, Y. Dai, M.H. Whangbo, Angew. Chem. Int. Ed. 52 (2013) 4810–4813.
[22] C.S. Guo, S. Yin, L. Huang, L. Yang, T. Sato, Chem. Commun. 47 (2011) 8853–8855.
[23] C.S. Guo, S. Yin, M. Yan, T. Sato, J. Mater. Chem. 21 (2011) 5099–5105.
[24] A. Hussain, L. Kihlborg, A. Klug, J. Solid State Chem. 25 (1978) 189–195.
[25] D.W. Lynch, R. Rosei, J. Solid State Chem. 8 (1973) 242–252.
[26] M. Green, Philos. Mag. B 51 (1985) 501–520.
[27] O.F. Schirmer, V. Wittwer, J. Electrochem. Soc. 124 (1977) 749–753.
[28] A.F. Huang, J. Song, L. Pan, X. Jia, Z. Li, J.J. Zou, X. Zhang, L. Wang, Nanoscale 6 (2014) 8865–8872.
[29] Z.F. Huang, J.J. Zou, L. Pan, S. Wang, X. Zhang, L. Wang, Appl. Catal. B 147 (2014) 167–174.
[30] Z.F. Huang, J. Song, L. Pan, X. Zhang, L. Wang, J. Zou, Adv. Mater. 27 (2015) 5309–5327.
[31] H. Tong, S. Ouyang, Y. Bi, N. Umezawa, M. Oshikiri, Jinhua Ye, Adv. Mater. 24 (2012) 229–251.
[32] L. Wang, Y. Yao, L. Sun, Y. Mao, W. Lu, S. Huang, W. Chen, Sep. Purif. Technol. 122 (2014) 449–455.
[33] L. Chen, S. Yamane, J. Mizukado, Y. Suzuki, S. Kutsuna, T. Uchimaru, H. Suda, Chem. Phys. Lett. 624 (2015) 87–92.
[34] Y. Yamakoshi, S. Aroua, T.D. Nguyen, Y. Iwamotoa, T. Ohnishi, Faraday Discuss. 173 (2014) 287–296.
[35] P. Wang, Y. Tang, Z. Dong, Z. Chen, T. Lim, J. Mater. Chem. A 1 (2013) 4718–4727.